remote sensing

MDPI

Technical Note

Performance of Multi-GNSS Real-Time UTC(NTSC) Time and Frequency Transfer Service Using Carrier Phase Observations

Pengfei Zhang [1,2,3], Rui Tu [1,4,5,*], Xiaochun Lu [1,4,5], Lihong Fan [1] and Rui Zhang [1]

[1] National Time Service Center, Chinese Academy of Sciences, Xi'an 710600, China; zhangpengfei@ntsc.ac.cn (P.Z.); luxc@ntsc.ac.cn (X.L.); fanlihong@ntsc.ac.cn (L.F.); zhangrui@ntsc.ac.cn (R.Z.)
[2] Key Laboratory of Time and Frequency Primary Standards, Chinese Academy of Sciences, Xi'an 710600, China
[3] State Key Laboratory of Geo-Information Engineering, Xi'an Research Institute of Surveying and Mapping, Xi'an 710054, China
[4] University of Chinese Academy of Sciences, Yu Quan Road, Beijing 100049, China
[5] Key Laboratory of Precision Navigation Positioning and Timing Technology, Chinese Academy of Sciences, Xi'an 710600, China
* Correspondence: turui@ntsc.ac.cn; Tel.: +86-029-8389-0246

Abstract: The technique of carrier phase (CP), based on the global navigation satellite system (GNSS), has proven to be a highly effective spatial tool in the field of time and frequency transfer with sub-nanosecond accuracy. The rapid development of real-time GNSS satellite orbit and clock determinations has enabled GNSS time and frequency transfer using the CP technique to be performed in real-time mode, without any issues associated with latency. In this contribution, we preliminarily built the prototype system of real-time multi-GNSS time and frequency transfer service in National Time Service Center (NTSC) of the Chinese Academy of Sciences (CAS), which undertakes the task to generate, maintains and transmits the national standard of time and frequency UTC(NTSC). The comprehensive assessment of the availability and quality of the service system were provided. First, we assessed the multi-GNSS state space representation (SSR) correction generated in real-time multi-GNSS prototype system by combining broadcast ephemeris through a comparison with the GeoForschungsZentrum (GFZ) final products. The statistical results showed that the orbit precision in three directions was smaller than 6 cm for global positioning system (GPS) and smaller than approximately 10 cm for BeiDou satellite system (BDS). The root mean square (RMS) values of clock differences for GPS were approximately 2.74 and 6.74 ns for the GEO constellation of BDS, 3.24 ns for IGSO, and 1.39 ns for MEO. The addition, the GLObal NAvigation Satellite System (GLONASS) and Galileo satellite navigation system (Galileo) were 4.34 and 1.32 ns, respectively. In order to assess the performance of real-time multi-GNSS time and frequency transfer in a prototype system, the four real-time time transfer links, which used UTC(NTSC) as the reference, were employed to evaluate the performance by comparing with the solution determined using the GFZ final products. The RMS could reach sub-nanosecond accuracy in the two solutions, either in the SSR or GFZ solution, or in GPS, BDS, GLONASS, and Galileo. The frequency stability within 10,000 s was 3.52×10^{-12} for SSR and 3.47×10^{-12} for GFZ and GPS, 3.63×10^{-12} for SSR and 3.53×10^{-12} for GFZ for BDS, 3.57×10^{-12} for SSR and 3.52×10^{-12} for GFZ for GLONASS, and 3.56×10^{-12} for SSR and 3.48×10^{-12} for GFZ for Galileo.

Keywords: time and frequency transfer; precise point positioning; multi-GNSS; UTC(NTSC); carrier phase observations

Citation: Zhang, P.; Tu, R.; Lu, X.; Fan, L.; Zhang, R. Performance of Multi-GNSS Real-Time UTC(NTSC) Time and Frequency Transfer Service Using Carrier Phase Observations. *Remote Sens.* **2021**, *13*, 4184. https://doi.org/10.3390/rs13204184

Academic Editors: Xingxing Li, Jacek Paziewski and Mattia Crespi

Received: 16 September 2021
Accepted: 14 October 2021
Published: 19 October 2021

1. Introduction

The global navigation satellite system (GNSS) has become an effective tool in time transfer. The global positioning system (GPS) was used for comparing a remote clock with the common-view (CV) technique back in the 1980s [1,2]. In this approach, two

GNSS receivers observed the common GNSS satellites to effectively eliminate some of the common errors, although most studies have proven that the CV approach can provide precision in the order of several nanoseconds [3,4]. The improvements in precise GNSS satellite orbit and clock products have led to the introduction of all-in-view (AV) and carrier-phase (CP) techniques. In the former, pseudorange measurement is still utilized, similar to the CV approach, as the pseudorange observation can directly measure the receiver clock offset between the GNSS receiver and satellite. Considering that GNSS carrier phase measurements are two orders of magnitude more precise than GNSS pseudorange data [5–8], the GNSS carrier-phase (CP) technique has been proposed for precise time transfer with the sub-nanosecond level precision [9–11]. The international GNSS service (IGS) provides three latency types of satellite orbit and clock products, such as ultra-rapid, rapid, and final products [12–15]. The latter two products, although high in quality, have latencies of approximately 17 h and 13 days after the end of the preceding observation and the last day of the week, respectively. This causes most applications, such as precise positioning and time transfer, to be limited to the post-processing mode. Ultra-rapid products have significantly inferior performance as compared to those derived from measurements [16]. To meet the growing demands for real-time high-precision time transfer applications, numerous studies are being undertaken to reduce the latency level of time transfer resolution. Petit et al. [17] employed the rapid products for GPS and GLObal NAvigation Satellite System (GLONASS) to generate Rapid Coordinated Universal Time (UTCr). Defraigne et al. [18] used the IGS real-time GPS products to carry out the CP time transfer campaign in near real time with low latency.

However, little research has focused on GNSS time and frequency transfer with real-time mode, particularly, the service system with new emerging GNSS (i.e., Galileo and BeiDou satellite system (BDS)) is still not clearly established. Therefore, in this contribution, the real-time multi-GNSS time and frequency transfer service prototype system was established at the National Time Service Center (NTSC) of the Chinese Academy of Sciences (CAS), which undertakes the task to generate, maintain and transmit the national standard of time and frequency. The real-time service (RTS) of multi-GNSS satellite products is herein also analyzed, and the availability and performance of real-time UTC (NTSC) multi-GNSS time transfer is subsequently assessed.

This article is organized as follows. We begin with a brief description of the model of real-time GNSS time and frequency transfer in prototype system, particular for the SSR products of satellite orbits and clocks and real-time data processing strategies. Afterward, we present issues related to the multi-GNSS SSR products and performance of time transfer in prototype system based on the experiment. Then, we discuss the real-time data processing procedure and evaluation of real-time multi-GNSS time transfer based on the experiment. Finally, the discussion and conclusion of our study are given.

2. Model of Real-Time GNSS Time and Frequency Transfer in Prototype System

Generally, although the ionosphere-free combination of dual-frequency GNSS carrier phase and code measurements converges much more slowly due to the poorer precision of ionosphere-free code observable [19,20], it was widely employed in the area of time and frequency transfer with CP technique for its simplicity of model. The observation model for the GNSS ionosphere-free code (P) and the carrier phase (Φ), can be written as [21–23]

$$\begin{cases} P = \rho + c \cdot (dt_r - dt_s) + T + \varepsilon_P \\ \Phi = \rho + c \cdot (dt_r - dt_s) + T + N + \varepsilon_\Phi \end{cases} \quad (1)$$

where ρ is the geometric distance receiver-satellite; N is the phase ambiguity; dt_s denotes the satellite clock offset; T is the tropospheric delay; ε_P and ε_Φ are the ionosphere-free noise for ionosphere-free code and carrier phase, respectively; and dt_r denotes the receiver clock offset. The hardware delay-induced GNSS receiver, antenna, and corresponding cables

can be calibrated as a whole parameter [24,25]. Therefore, we can consider the unknown parameters in Equation (1), which are written as:

$$\overline{X} = \left[x, y, z, dt_r, T_{trop}, N\right]^T \tag{2}$$

where the receiver clock offsets the clock difference between external atomic clock and GNSS timescale (*GNSST*) [26], which can be expressed as:

$$dt_r^A = Time(A) - GNSST \tag{3}$$

A time transfer operation between the two atomic clocks, $Time(A)$ and $Time(B)$, connected to their GNSS receivers, is called a time link, which is denoted as $Time(A) - Time(B)$, the operation of time transfer can be written as:

$$Time(A) - Time(B) = dt_r^A - dt_r^B \tag{4}$$

2.1. SSR Products of Satellite Orbits and Clocks

Currently, the practice of accessing GNSS data and differential correction using the Networked Transport of Radio Technical Commission for Maritime Services (RTCM) through Internet Protocol (NTRIP) [27] is widely used in numerous applications. The IGS analysis centers (ACs) have provided SSR format correction for real-time products [28,29], of which the refereeing is the International Terrestrial Reference Frame 2008 (ITRF08). Therefore, the NTSC of the Chinese Academy of Sciences (CAS) has also generated and broadcasted real-time precise orbits and a clock correction with the SSR format. Since the orbit correction is written as three directions with satellite-fixed coordinate system, it should be converted to Earth-centered Earth-fixed reference frame (ECEF) system during the data processing. Regarding the clock correction, this is considered as an offset to the broadcast satellite clock. As the SSR correction of the orbit and clock refers to broadcast navigation data, one should be compatible with the current navigation message with issue of the data *IODE* during the time and frequency data processing. Therefore, the SSR correction parameters can be summarized as follows:

$$\Delta_{SSR}(t_0,\ IODE) = \left(\delta \boldsymbol{O}_r, \delta \boldsymbol{O}_a, \delta \boldsymbol{O}_c, \delta \dot{\boldsymbol{O}}_r, \delta \dot{\boldsymbol{O}}_a, \delta \dot{\boldsymbol{O}}_c, C_0, C_1, C_2\right) \tag{5}$$

where *IODE* denotes the issue of the data, and $(\delta \boldsymbol{O}_r, \delta \boldsymbol{O}_a, \delta \boldsymbol{O}_c)$ and $(\delta \dot{\boldsymbol{O}}_r, \delta \dot{\boldsymbol{O}}_a, \delta \dot{\boldsymbol{O}}_c)$ are the correction and the change rate at time t_0 in the three satellite-fixed coordinate system components, respectively. Furthermore, (C_0, C_1, C_2) denotes the polynomial coefficients for calculating clock correction.

The SSR correction of satellite orbit is applied as following procedures [30,31]:

First, the orbit corrections at epoch t are calculated as follows:

$$\delta \boldsymbol{O} = \begin{bmatrix} \delta \boldsymbol{O}_r \\ \delta \boldsymbol{O}_a \\ \delta \boldsymbol{O}_c \end{bmatrix} + \begin{bmatrix} \delta \dot{\boldsymbol{O}}_r \\ \delta \dot{\boldsymbol{O}}_a \\ \delta \dot{\boldsymbol{O}}_c \end{bmatrix} (t - t_0) \tag{6}$$

Thereafter, the coordinate system is transformed to ECEF corrections as follows:

$$\delta \boldsymbol{X} = \begin{bmatrix} \boldsymbol{e}_r & \boldsymbol{e}_a & \boldsymbol{e}_c \end{bmatrix} \delta \boldsymbol{O} \tag{7}$$

where $\boldsymbol{e}_a = \frac{\dot{r}}{|\dot{r}|}$, $\boldsymbol{e}_c = \frac{r \times \dot{r}}{|r \times r|}$, and $\boldsymbol{e}_r = \boldsymbol{e}_a \times \boldsymbol{e}_c$. Finally, the precise orbits, $\boldsymbol{X}$, with broadcast orbits, $\boldsymbol{X_b}$ are determined as follows:

$$\boldsymbol{X} = \boldsymbol{X_b} - \delta \boldsymbol{X} \tag{8}$$

The precise clock corrections can be determined at epoch t as:

$$\delta k = C_0 + C_1(t - t_0) + C_2(t - t_0)^2 \quad (9)$$

$$t = t_b - \frac{\delta k}{c} \quad (10)$$

2.2. Structure of Real-Time Prototype System

During data processing, the real-time multi-GNSS observation streams in the IGS and Multi-GNSS Experiment (MGEX) are collected to generate real-time precise orbit and clock products in the prototype system of real-time multi-GNSS time and frequency transfer service in NTSC. The multi-GNSS products were distributed through the internet, based on the SSR format. The SSR correction, combined with the corresponding individual GNSS broadcast ephemeris, was used to recover the precise satellite orbit and clock, which were then transmitted to the GNSS time transfer software (PTTSol) [32,33]. The real-time GNSS data of at least of two stations with time and frequency references were also collected using NTRIP caster software. Generally, one of the two stations can be connected to the time and frequency reference UTC(k) in a time laboratory, which is well maintained and has participated in UTC computation in the International Bureau of Weights and Measures (BIPM) [34,35]. Here, k refers to the abbreviation of time laboratory in BIPM. All the prerequisites were met when the real-time raw GNSS data for time and frequency transfer were collected; these were then used in the GNSS time transfer software. The prototype system of real-time GNSS time transfer service in NTSC is briefly summarized in Figure 1, which mainly includes three parts. The part 1 is the real-time orbit and clock determined block, of which the main functions are collecting the real-time global GNSS station observation data, real-time satellite orbit and clock determination in satellite-fixed coordinate system. Part 2 is the real-time satellite orbit and clock recovery block, of which the coordinate system is an ECEF system. The last part is the time and frequency transfer block, when combining the real-time satellite products and user's GNSS data, the solution of real-time time transfer can be determined. Table 1 details the data processing strategies used in this part.

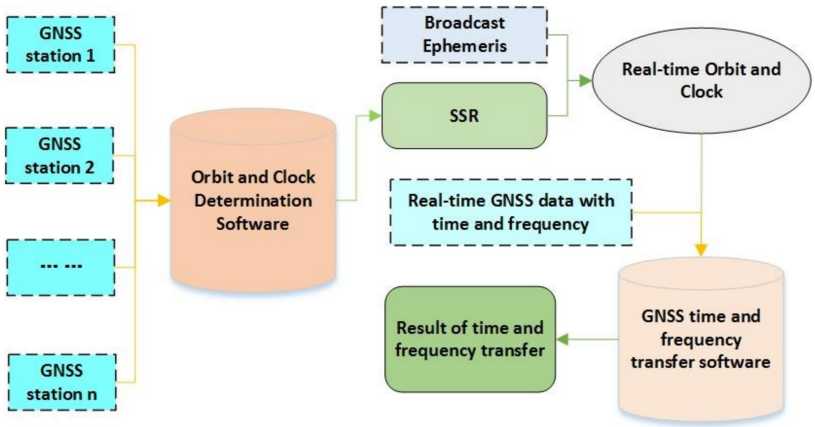

Figure 1. Prototype system of real-time multi-GNSS time transfer service.

Table 1. The models and strategies adopted in the real-time GNSS prototype system.

Item	Models/Strategies
Observations	Pseudorange and carrier phase observation
Constellations and Frequency	BDS(B1/B2), GPS(L1/L2), Galileo(E1/E5a),GLONASS(L1/L2)
Satellite orbit and clock	Real-time GNSS products derived from NTSC
Cycle slip of carrier phase	Geometry-free (GF) + Hatch–Melbourne–Wübbena (HMW)
Tropospheric delay	Initial model(Saastamoinen) + random-walk process [36]
Priori standard deviation	0.3 m (Pseudorange), 0.003 m(Carrier phase) [37–39]
Phase wind-up	Model-corrected
Receiver clock offset	Estimated as white noise [40]
Tidal effects	Solid tide, pole tide, ocean loading
Phase ambiguities	Float solution [41]
Estimator	Least square estimation in sequential mode

3. Results

3.1. Multi-GNSS SSR Products in Prototype System

As GNSS satellite products are primary prerequisites for time transfer, which slightly affects the capacity of the system service, we first assessed the quality of real-time multi-GNSS SSR products in prototype system by referencing to the GFZ final precise product, available from GFZ for day of year (DOY) 346–349, 2019. The real-time streams of observation data of IGS/MGEX ground tracking stations distributed in most of the areas of the world were collected via NTRIP caster software in RTCM format. Most stations can track GPS signals; however, the number of stations that can receive BDS, GLONASS, and Galileo is limited. Raw data from approximately 86 stations were used during this period, and all these stations could track GPS satellite signals, and most stations are able to track GLONASS (81). Approximately 73 and 55 stations are available for the Galileo, and BeiDou, respectively. The locations of the stations are depicted in Figure 2.

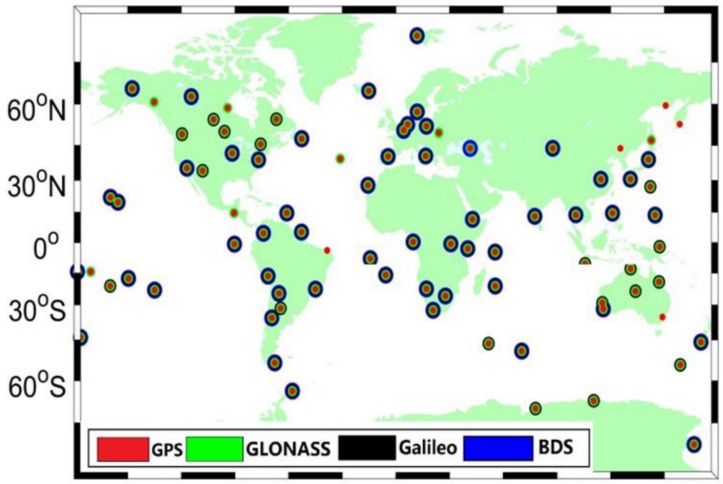

Figure 2. Distribution of real-time GNSS stations in NTSC time and frequency transfer prototype system for products determine.

Figure 3 and Table 2 show the average root mean square (RMS) in the three components of orbits calculated for real-time multi-GNSS, with reference to the GFZ's final products. The limited tracking stations for BDS leads to its low accuracy for orbits. For GLONASS, the orbit accuracy was lower than that of GPS, owing to its float ambiguity resolution.

The RMS and STD of the real-time clock products compared to the GFZ final products were employed as the indicator to assess the clock performance. The former reflects the compliance of the clock correction, while the latter represents the precision of the clock. Figure 4 and Table 2 present the average RMS and STD values for each satellite from DOY 346 to 349 in 2019. The average RMS values of GPS satellites are under 4 ns.

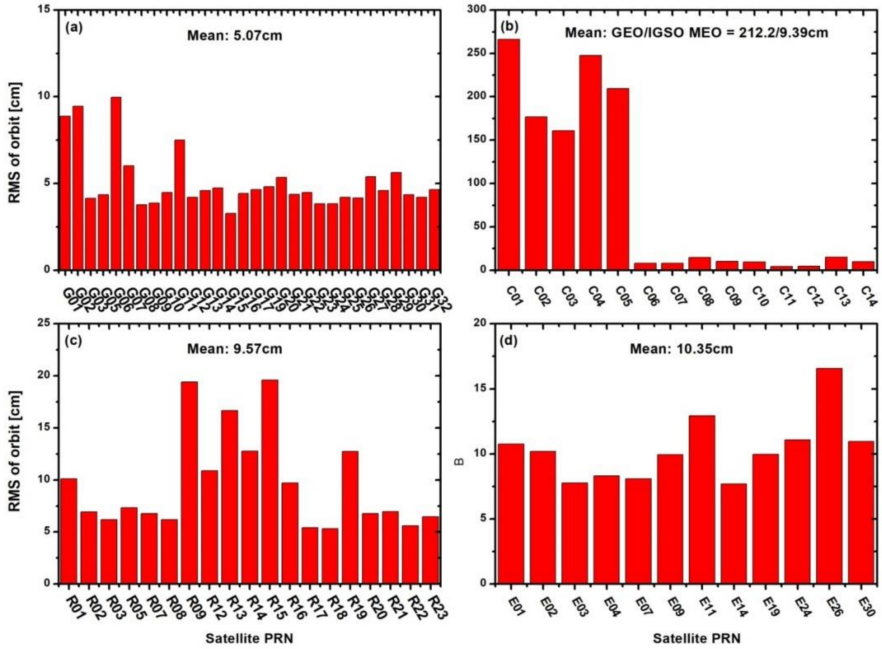

Figure 3. Average RMS of orbits in three directions, calculated for real-time multi-GNSS compared to GFZ's final products: (**a**) GPS; (**b**) BDS; (**c**) GLONASS; (**d**) GALILEO.

Table 2. Mean values of RMS and STD of orbit and clock determination.

GNSS	Orbit	Clock	
	RMS (cm)	RMS (ns)	STD (ns)
GPS	5.07	2.74	0.35
BDS(GEO)	212.20	6.74	0.55
BDS(IGSO)	10.27	3.24	0.31
BDS(MEO)	8.50	1.39	0.24
GLONASS	9.57	4.34	0.42
Galileo	10.35	1.32	0.30

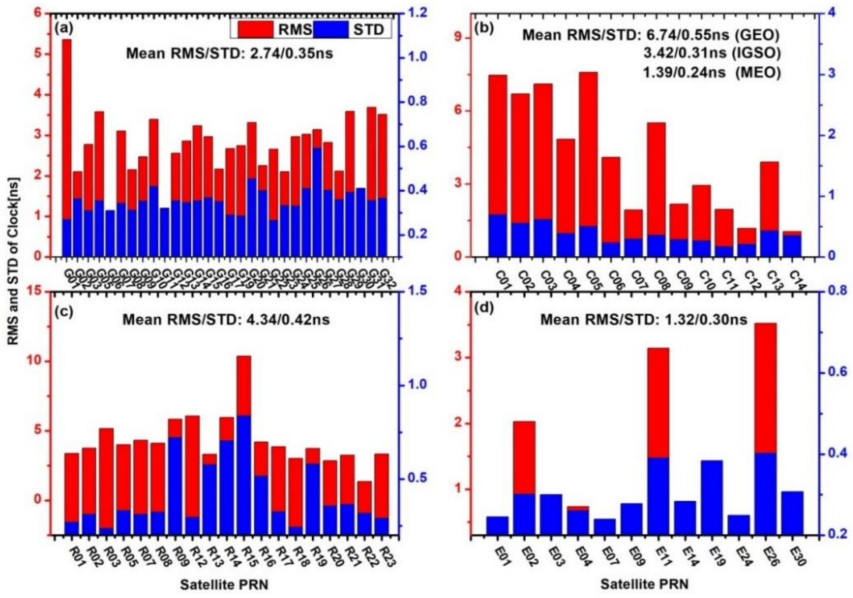

Figure 4. Average RMS and STD values real-time calculation compared with GFZ final products for DOY 346 to 349, 2019. (**a**) GPS; (**b**) BDS; (**c**) GLONASS; (**d**) Galileo.

3.2. Evaluation of Real-Time GNSS Time Transfer

Five stations that can track multi-GNSS signals were collected to assess the performance of time transfer service in the NTSC prototype system. Two of these stations were equipped with cesium clocks, one was hydrogen clock and the last one was crystal clock steered to a hydrogen maser, which was placed in a different room. Station NTP3 was connected to the time and frequency reference UTC(NTSC); it was traceable to UTC within 5 ns for the past two years. Therefore, four time links were established, and UTC(NTSC) was selected as the reference. Detailed information of the stations used is provided in Table 3. In order to assess the performance of the prototype system for real-time GNSS time transfer service, we also employed the GFZ final satellite products to determine the time and transfer result, of which the solution denotes as "GFZ" solution, while the solution in the prototype system is denoted as "SSR" solution, hereafter, in this paper. Notably, the RMS values of the smooth residuals and frequency stability were numerical evaluation indicators in the area of time transfer.

Table 3. Detailed information about the five stations.

Name	Receiver	Antenna	Frequency Standard	Location
NPT3	Sept Polarx4TR	SEPCHOKE_MC	UTC(NTSC)	34.37°N, 109.22°E
GMSD	Trimble NetR9	TRM59800	Cesium	30.56°N, 131.02°E
YARR	Sept Polarx5	LEIATT504	Cesium	29.05°S, 115.35°E
HOB2	Sept Polarx5	AOAD	H-maser	42.80°S, 147.44°E
NNOR	Sept Polarx5TR	SEPCHOKE_B3E6	Slaved Crystal	31.05°S, 116.19°E

3.2.1. GPS

Figure 5 depicts the GPS time transfer results for SSR and GFZ solutions. Notably, the variations in time transfer for both the solutions at all four time links show good consistency, although different types of atomic clocks were used. This indicates that real-time SSR products can be effectively employed in the domain of time transfer.

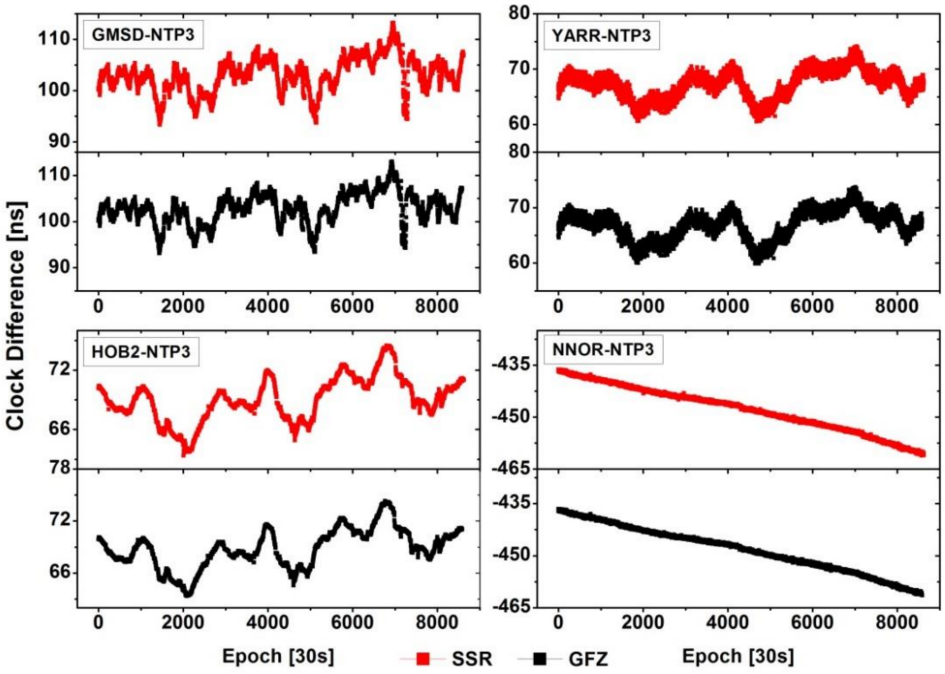

Figure 5. GPS results for SSR and GFZ solutions.

For the noise levels of the different time links, the RMS values of the smooth residuals of GPS result are provided in Table 4. These RMS values reached the sub-nanosecond

level of accuracy for both solutions. The RMS in HOB2–NTP3 and NNOR–NTP3 are significantly smaller than the other two time links. This is likely because they are equipped with different types of atomic clocks; the former two use a hydrogen maser, whereas the latter two use a cesium clock Furthermore, the SSR solutions reached 0.500 ns for those time links, which is slightly lower than the GFZ solutions (0.0491 ns).

Table 4. RMS of GPS results for the time links (ns).

GPS Solutions	GMSD–NTP3	YARR–NTP3	HOB2–NTP3	NNOR–NTP3
SSR (ns)	0.939	0.638	0.224	0.200
GFZ (ns)	0.908	0.634	0.221	0.200

Figure 6 shows the Allen deviation (ADEV) values of the two solutions. The SSR solution exhibits slightly worse performance as compared to the GFZ for the four time links, particularly when the average time intervals are within 10,000 s. The corresponding mean values for the four time links were determined: (2.88, 2.71) $\times 10^{-12}$ for (SSR, GFZ) at the GMSD–NTP3 time link, (8.08, 8.09) $\times 10^{-12}$ for (SSR, GFZ) at YARR–NTP3, (8.32, 7.46) $\times 10^{-13}$ for (SSR, GFZ) at HOB2–NTP3, for (SSR, GFZ) at the NNOR–NTP3 time link, respectively, and (2.29, 2.34) $\times 10^{-12}$.

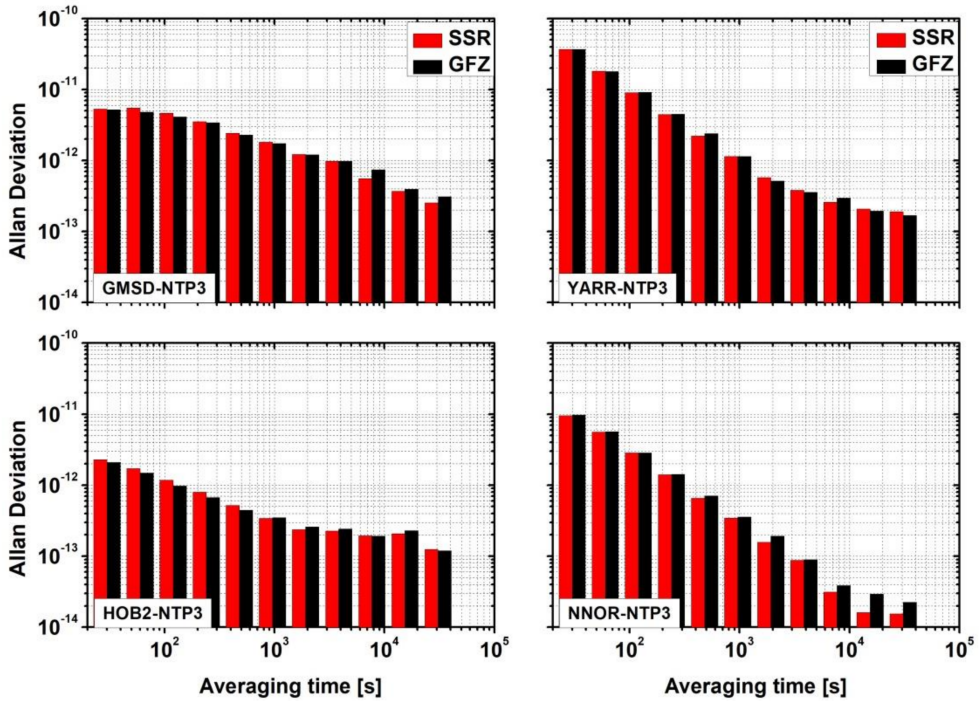

Figure 6. GPS Allan deviation (ADEV) for SSR and GFZ solutions.

3.2.2. BDS

Figure 7 shows the time transfer results using BDS observation for the two solutions. One can note that both the SSR and GFZ products can provide reliable time transfer results. The variations in the time transfer during the entire experiment show good consistency at all four time links. The RMS values of the smoothed residual are summarized in Table 5. The character of the RMS among the different time links for the two solutions is generally similar at the nanosecond level of accuracy. Furthermore, the RMS in the two cesium clock time links is larger than that of the two time links with hydrogen masers. The mean RMS values were 0.515 ns for the SSR solutions and 0.507 ns for the GFZ solutions.

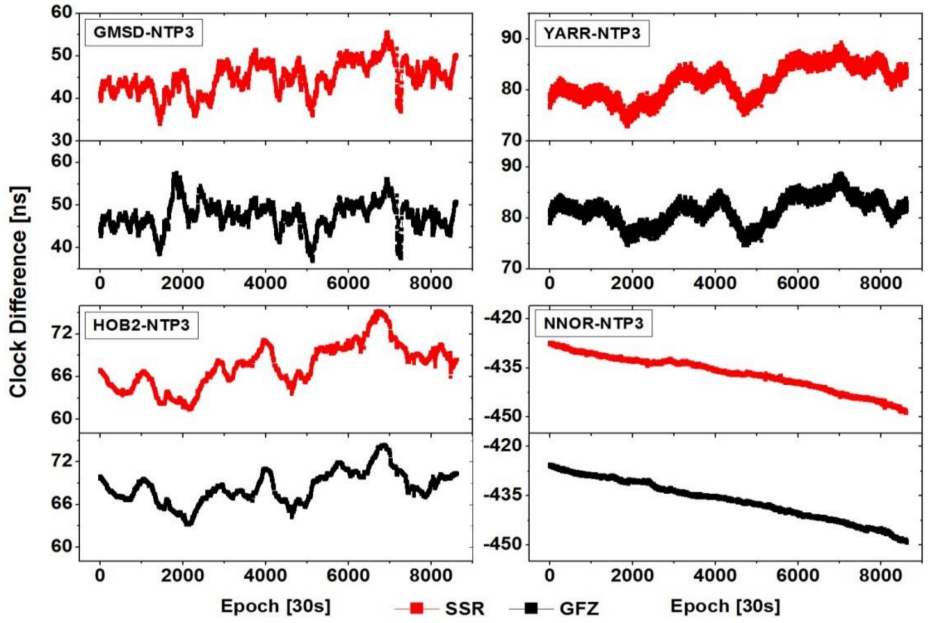

Figure 7. BDS results for SSR and GFZ solutions.

Table 5. RMS of BDS results for the time links (ns).

BDS Solutions	GMSD–NTP3	YARR–NTP3	HOB2–NTP3	NNOR–NTP3
SSR (ns)	0.955	0.639	0.260	0.205
GFZ (ns)	0.963	0.636	0.228	0.203

Figure 8 shows the frequency stability for the two solutions. The SSR solution showed inferior performance as compared to GFZ, and the average stability values within 10,000 s were (2.95, 3.01) $\times$ 10^{-12} for (SSR, GFZ) at GMSD–NTP3; (8.09, 8.07) $\times$ 10^{-12} for (SSR, GFZ) at YARR–NTP3; (1.16, 0.766) $\times$ 10^{-12} for (SSR, GFZ) at HOB2–NTP3; and (2.33, 2.26) $\times$ 10^{-12} for (SSR, GFZ) for NNOR–NTP3, respectively.

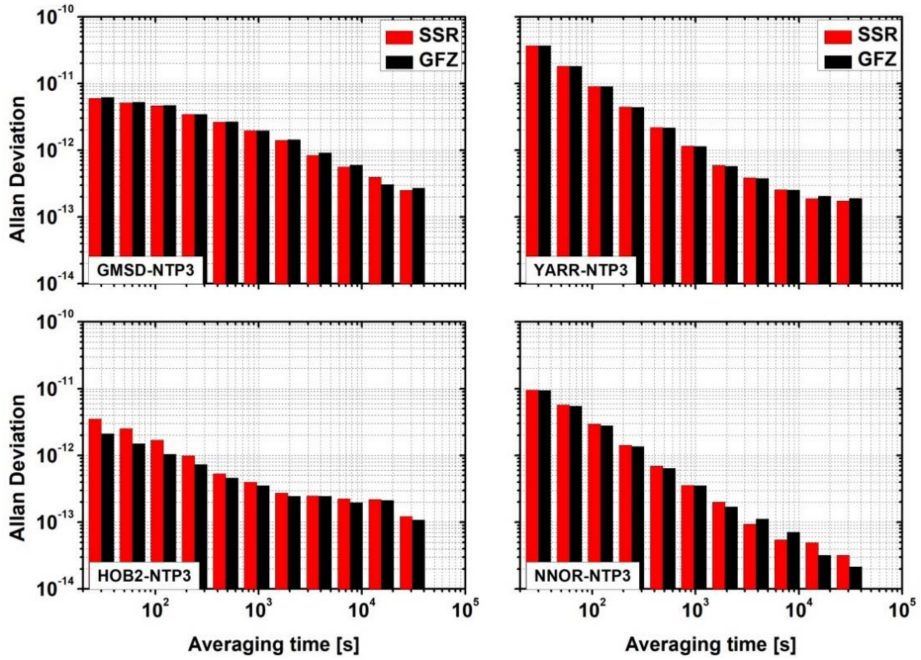

Figure 8. BDS Allan deviation (ADEV) for SSR and GFZ solutions.

3.2.3. GLONASS

Figure 9 shows the time transfer results using GLONASS observation for the two solutions. Similar trends were observed for the SSR and GFZ solutions, although they were equipped with different types of atomic clocks. Similarly, the RMS values of the smoothed residuals of the two solutions are summarized in Table 6. For these time links, the RMS in the SSR solutions are slightly lower than in the GFZ, and the averaged RMS values were 0.504 ns, 0.494 ns for the SSR and GFZ solutions, respectively. Furthermore, by comparing the GPS and BDS results, the RMS values in GLONASS are generally higher than BDS but lower as compared to GPS.

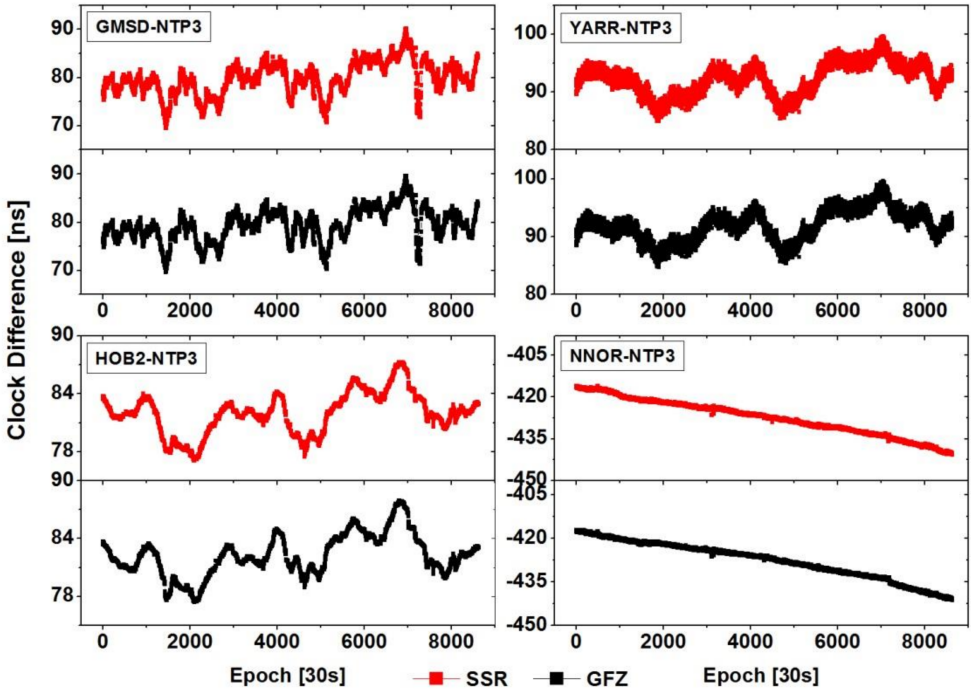

Figure 9. GLONASS results for SSR and GFZ solutions.

Table 6. RMS of GLONASS results for the time links (ns).

GLONASS Solutions	GMSD–NTP3	YARR–NTP3	HOB2–NTP3	NNOR–NTP3
SSR (ns)	0.934	0.643	0.222	0.216
GFZ (ns)	0.913	0.633	0.226	0.204

Figure 10 provides the frequency stability comparison for the two solutions in GLONASS. Similarly, the SSR values are in good agreement with the GFZ solution at different time intervals of the different time links, although the performance of SSR is slightly inferior as compared to the GFZ solution. The average stability values within 10,000 s were (2.86, 2.87) $\times 10^{-12}$ for (SSR, GFZ) at GMSD–NTP3; (8.08, 8.06) $\times 10^{-12}$ for (SSR, GFZ) at YARR–NTP3; (7.69, 7.62) $\times 10^{-13}$ for (SSR, GFZ) at HOB2–NTP3; and (2.56, 2.38) $\times 10^{-12}$ for (SSR, GFZ) at NNOR–NTP3, respectively.

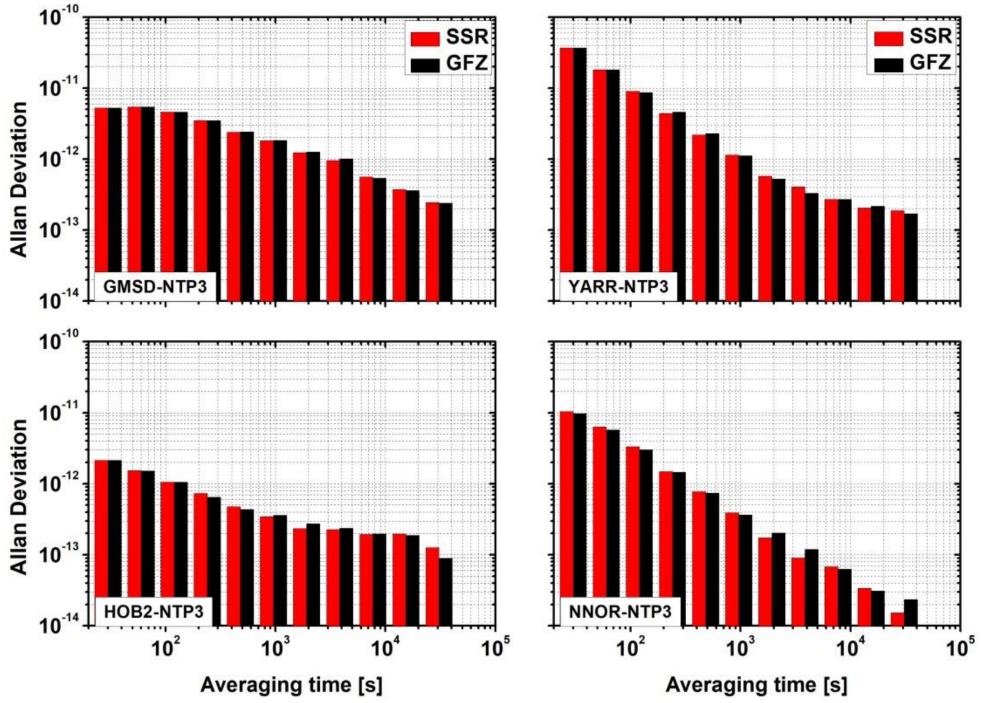

Figure 10. GLONASS Allan deviation (ADEV) for SSR and GFZ solutions.

3.2.4. Galileo

Figure 11 illustrates the results using Galileo observation for the SSR and GFZ solutions at all four links. Both the SSR and GFZ solutions can provide the time transfer result, and their variations show good consistency at the four different time links, although different types of atomic clocks were used. Table 7 gives the RMS values, and they are analogous, although the averaged values were 0.510 and 0.497 ns for SSR and GFZ solutions, respectively.

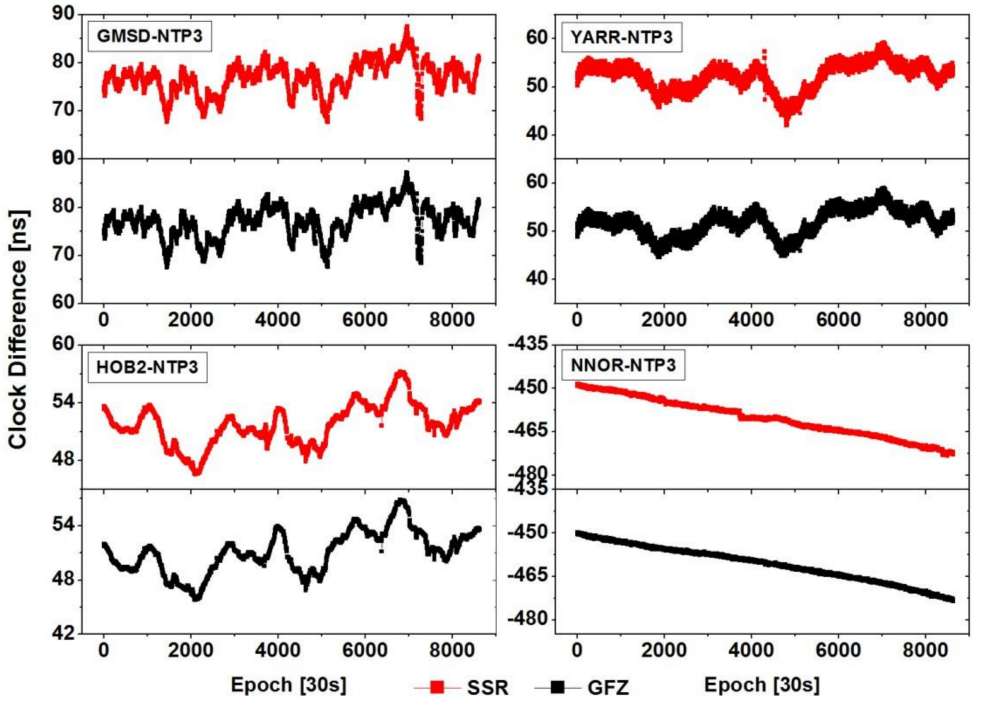

Figure 11. Galileo results for SSR and GFZ solutions.

Table 7. RMS of Galileo results for the time links (ns).

Galileo Solutions	GMSD–NTP3	YARR–NTP3	HOB2–NTP3	NNOR–NTP3
SSR (ns)	0.945	0.648	0.231	0.217
GFZ (ns)	0.936	0.636	0.223	0.194

Figure 12 shows the frequency stability comparison using Galileo observation between the two solutions. The SSR shows better agreement with the GFZ solution at different time intervals, although the performance of the SSR solution was slightly inferior as compared to the GFZ solution. The average stability values within 10,000 s were (2.93, 2.85) $\times 10^{-12}$ for (SSR, GFZ) at GMSD–NTP3, (8.09, 8.07) $\times 10^{-12}$ for (SSR, GFZ) at YARR–NTP3, (8.15, 7.57) $\times 10^{-13}$ for (SSR, GFZ) at HOB2–NTP3, and (2.29, 2.25) $\times 10^{-12}$ for (SSR, GFZ) for the NNOR–NTP3 time links, respectively.

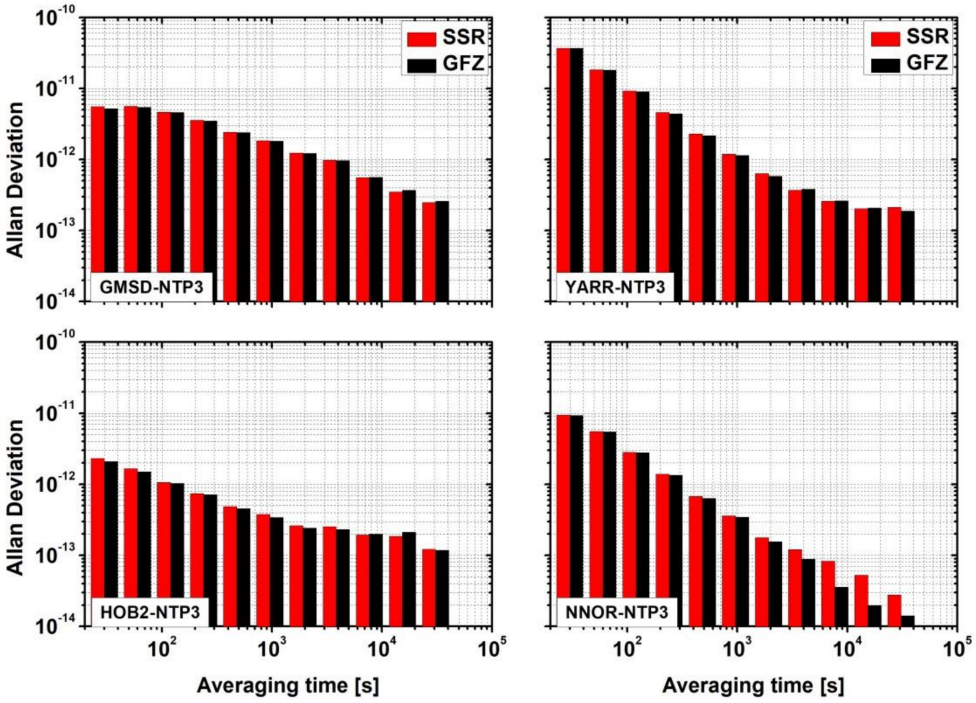

Figure 12. Galileo Allan deviation (ADEV) for SSR and GFZ solutions.

4. Discussion

The real-time time and frequency transfer is essential for UTC comparison and traceability services. At present, few studies have focused on the GNSS time and frequency transfer with real-time mode, particularly for BDS and Galileo system. Therefore, the prototype system of a real-time multi-GNSS time and frequency transfer service was preliminarily established in NTSC. We first introduced the basic structure of prototype system and analyzed its performance from real-time satellite products and real-time multi-GNSS time transfer.

For the satellite orbit and clock products, the RMS and STD of satellite orbit and clock in prototype system is given in Figures 3 and 4 by comparing the GFZ final satellite products. The mean values of RMS and STD of the orbit and clock are also summarized in Table 2.

In order to further verify the stability and the precision of the real-time multi-GNSS time and frequency transfer in the prototype system, four time links referring UTC(NTSC) were established. The GPS, BDS, GLONASS and Galileo time transfer results are given in Figures 5, 7, 9 and 11, respectively. The characters of time transfer in a prototype system

solutions are similar to the GFZ solutions with final satellite products. In the numerical statistical indicators of noise level (Tables 4–7) and frequency stability (Figures 6, 8, 10 and 12), the values were in good agreement, although the relative precision of individual GNSS solution and stability of the individual clocks varied considerably. This means that the results in the prototype system of real-time multi-GNSS time and frequency transfer service in NTSC is available and credible, which can provide the little latency time transfer service (only network communication delay) with a sub-nanosecond accuracy level.

This study proposes only the first step of this research, and several topics still require further investigation in our near future work, for example: how to combine the four GNSSs in real-time mode for time and frequency transfer in the prototype system; how to provide the carrier phase ambiguity resolution service for time users; and how hardware calibrates in the time link based on multi-system time and frequency transfer.

5. Conclusions

The prototype system of real-time multi-GNSS time and frequency transfer service was preliminarily established in NTSC, of which the time and frequency reference UTC(NTSC) is traceable to UTC. The real-time experimental results show that the performances in the prototype system are comparable to the GFZ final solution. Conclusions can be summarized as follows:

(1) Regarding the satellite orbit products, GPS solution in prototype system performed the best in the averaged RMS values in the three directions when compared to the BDS, GLONASS, and Galileo systems. For the available satellites, the mean values were 5.07 cm for GPS, 212 cm for the GEO constellation of BDS, 9.39 cm for the IGSO and MEO constellations of BDS, 9.57 cm for GLONASS, and 10.35 cm for Galileo.

(2) For the clock products in the prototype system, the mean RMS values for all the satellites were 2.74 ns for GPS, 6.74 ns for the GEO constellation of BDS, 3.24 ns for IGSO, and 1.39 ns for MEO. The mean value for GLONASS was 4.34 ns, whereas that of Galileo was 1.32 ns.

(3) With respect to the time transfer service, the RMS values of the smoothed residuals at all time links could reach the sub-nanosecond accuracy level, regardless of whether the prototype system or GFZ solution was used, in GPS, BDS, GLONASS, and Galileo. Overall, the prototype system solutions are similar to that of GFZ regarding the noise level of the time link. For the ADEV of the time links, the characters of the prototype system solution are also equivalent to that of GFZ at different time intervals for the four time links. The frequency stability within 10,000 s was 3.52×10^{-12} for SSR and 3.47×10^{-12} for GFZ and GPS. For the four time links, it was 3.63×10^{-12} for SSR and 3.53×10^{-12} for GFZ for BDS, 3.57×10^{-12} for SSR and 3.52×10^{-12} for GFZ for GLONASS, and 3.56×10^{-12} for SSR and 3.48×10^{-12} for GFZ for Galileo.

Author Contributions: P.Z. and R.T. conceived and designed the experiments; P.Z. performed the experiments, analyzed the data, and wrote the paper. X.L., L.F. and R.Z. contributed to discussions and revisions. All authors have read and agreed to the published version of the manuscript.

Funding: This research was funded by National Natural Science Foundation of China (grant no: 11903040, 41674034, 41974032) and Chinese Academy of Sciences (CAS) programs of "High Level Talents", "The Frontier Science Research Project" (grant no: QYZDB-SSW-DQC028), "Western young scholars" (grant no.: XAB2019B21), China Postdoctoral Science Foundation (grant no: 2020M683763).

Institutional Review Board Statement: Not applicable.

Informed Consent Statement: Not applicable.

Data Availability Statement: The datasets analyzed in this study are managed by the MGEX and National Time Service Center, Chinese Academy of Sciences, which can be available on request from the corresponding author.

Acknowledgments: Many thanks goes to the IGS MGEX for providing multi-GNSS ground tracking data, precise orbit and clock products.

Conflicts of Interest: The authors declare no conflict of interest.

References

1. Allan, D.W.; Thomas, C. Technical directives for standardization of GPS time receiver software. *Metrologia* **1994**, *31*, 69–79. [CrossRef]
2. Allan, D.W.; Weiss, M. Accurate time and frequency transfer during common-view of a GPS satellite. In Proceedings of the 1980 IEEE Frequency Control Symposium, Philadelphia, PA, USA, 28–30 May 1980; pp. 334–356.
3. Petit, G.; Jiang, Z. GPS All in View time transfer for TAI computation. *Metrologia* **2008**, *45*, 35–45. [CrossRef]
4. Jiang, Z.; Lewandowski, W. Use of GLONASS for UTC time transfer. *Metrologia* **2012**, *49*, 57–61. [CrossRef]
5. Defraigne, P.; Bruyninx, C.; Guyennon, N. PPP and phase only GPS frequency transfer. In Proceedings of the IEEE International Frequency Control Symposium Jointly with the 21st European Frequency and Time Forum (EFTF' 07), Geneva, Switzerland, 29 May–1 June 2007; pp. 904–908.
6. Defraigne, P.; Baire, Q. Combining GPS and GLONASS for time and frequency transfer. *Adv. Space Res.* **2011**, *47*, 265–275. [CrossRef]
7. Defraigne, P.; Bruyninx, C. On the link between GPS pseudorange noise and day-boundary discontinuities in geodetic time transfer solutions. *GPS Solut.* **2007**, *11*, 239–249. [CrossRef]
8. Delporte, J.; Mercier, F.; Laurichesse, D.; Galy, O. GPS carrier phase time transfer using single difference integer ambiguity resolution. *Int. J. Navig. Obs.* **2008**, *2008*, 273785. [CrossRef]
9. Guang, W.; Dong, S.; Wu, J.; Zhang, Y.; Yuan, S. Progress of BeiDou time transfer at NTSC. *Metrologia* **2018**, *55*, 175–187. [CrossRef]
10. Zhang, P.; Tu, R.; Gao, Y.; Cai, H. Day-Boundary Discontinuity in GPS Carrier-Phase Time Transfer Using a Geodetic Data Solution Strategy. *J. Surv. Eng.* **2019**, *145*, 04018013. [CrossRef]
11. Tu, R.; Zhang, P.; Zhang, R.; Liu, J.; Lu, X. Modeling and Assessment of Precise Time Transfer by Using BeiDou Navigation Satellite System Triple-Frequency Signals. *Sensors* **2018**, *18*, 1017. [CrossRef] [PubMed]
12. Li, X.; Ge, M.; Dai, X.; Ren, X.; Fritsche, M.; Wickert, J.; Schuh, H. Accuracy and reliability of multi-GNSS real-time precise positioning: GPS, GLONASS, BeiDou, and Galileo. *J. Geod.* **2015**, *89*, 607–635. [CrossRef]
13. Montenbruck, O.; Steigenberger, P.; Prange, L.; Deng, Z.; Zhao, Q.; Perosanz, F.; Romero, I.; Noll, C.; Stürze, A.; Weber, G.; et al. The Multi-GNSS Experiment (MGEX) of the International GNSS Service (IGS)–Achievements, prospects and challenges. *Adv. Space Res.* **2017**, *59*, 1671–1697. [CrossRef]
14. Gioia, C.; Borio, D.; Angrisano, A.; Gaglione, S.; Fortuny-Guasch, J. A Galileo IOV assessment: Measurement and position domain. *GPS Solut.* **2015**, *19*, 187–199. [CrossRef]
15. Uhlemann, M.; Gendt, G.; Ramatsch, M.; Deng, Z. GFZ Global Multi-GNSS Network and Data Processing Results. In *IAG 150 Years. International Association of Geodesy Symposia*; Rizos, C., Willis, P., Eds.; Springer: Cham, Switzerland, 2015; Volume 143, pp. 673–679.
16. Hadas, T.; Bosy, J. IGS RTS precise orbits and clocks verification and quality degradation over time. *GPS Solut.* **2015**, *19*, 93–105. [CrossRef]
17. Petit, G.; Arias, F.; Harmegnies, A.; Panfilo, G.; Tisserand, L. UTCr: A rapid realization of UTC. *Metrologia* **2013**, *51*, 33–39. [CrossRef]
18. Defraigne, P.; Aerts, W.; Pottiaux, E. Monitoring of UTC(k)'s using PPP and IGS real-time products. *GPS Solut.* **2015**, *19*, 165–172. [CrossRef]
19. Teunissen. *GNSS Precise Point Positioning. Chapter 20 in Position, Navigation, and Timing Technologies in the 21st Century: Integrated Satellite Navigation, Sensor Systems, and Civil Applications*; Jade Morton, Y., Ed.; John Wiley & Son: Hoboken, NJ, USA, 2021.
20. An, X.D.; Meng, X.L.; Jiang, W.P. Multi-constellation GNSS precise point positioning with multi-frequency raw observations and dual-frequency observations of ionospheric-free linear combination. *Satell. Navig.* **2020**, *1*, 7. [CrossRef]
21. Tavella, P.; Petit, G. Precise time scales and navigation systems: Mutual benefits of timekeeping and positioning. *Satell. Navig.* **2020**, *1*, 10. [CrossRef]
22. Petit, G.; Defraigne, P. The performance of GPS time and frequency transfer: Comment on 'A detailed comparison of two continuous GPS carrier phase time transfer techniques'. *Metrologia* **2016**, *53*, 1003–1008. [CrossRef]
23. Afifi, A.; El-Rabbany, A. Performance Analysis of Several GPS/Galileo Precise Point Positioning Models. *Sensors* **2015**, *15*, 14701–14726. [CrossRef] [PubMed]
24. Zhang, P.; Tu, R.; Zhang, R.; Gao, Y.; Cai, H. Combining GPS, BeiDou, and Galileo Satellite Systems for Time and Frequency Transfer Based on Carrier Phase Observations. *Remote Sens.* **2018**, *10*, 324. [CrossRef]
25. Rovera, G.D.; Torre, J.M.; Sherwood, R.; Abgrall, M.; Courde, C.; Laas-Bourez, M.; Uhrich, P. Link calibration against receiver calibration: An assessment of GPS time transfer uncertainties. *Metrologia* **2014**, *51*, 476–490. [CrossRef]
26. Zhang, P.; Tu, R.; Gao, Y.; Guang, W.; Zhang, R.; Cai, H. Study of time link calibration based on GPS carrier phase observation. *IET Radar Sonar Navig.* **2018**, *12*, 1330–1335. [CrossRef]
27. Nicolini, L.; Caporali, A. Investigation on Reference Frames and Time Systems in Multi-GNSS. *Remote Sens.* **2018**, *10*, 80. [CrossRef]
28. Wang, L.; Li, Z.; Ge, M.; Neitzel, F.; Wang, Z.; Yuan, H. Validation and Assessment of Multi-GNSS Real-Time Precise Point Positioning in Simulated Kinematic Mode Using IGS Real-Time Service. *Remote Sens.* **2018**, *10*, 337. [CrossRef]

29. Wang, Z.; Li, Z.; Wang, L.; Wang, X.; Yuan, H. Assessment of Multiple GNSS Real-Time SSR Products from Different Analysis Centers. *ISPRS Int. J. Geo-Inf.* **2018**, *7*, 85. [CrossRef]
30. Liu, Z.; Wang, J. Realization and analysis of real-time precise point positioning based on SSR broadcast ephemeris corrections. *Sci. Surv. Mapp.* **2014**, *39*, 15–19.
31. Janicka, J.; Tomaszewski, D.; Rapinski, J.; Jagoda, M.; Rutkowska, M. The Prediction of Geocentric Corrections during Communication Link Outages in PPP. *Sensors* **2020**, *20*, 602. [CrossRef]
32. Pelc-Mieczkowska, R.; Tomaszewski, D. Space State Representation Product Evaluation in Satellite Position and Receiver Position Domain. *Sensors* **2020**, *20*, 3791. [CrossRef]
33. Zhang, P.; Tu, R.; Gao, Y.; Liu, N.; Zhang, R. Evaluation of carrier-phase precise time and frequency transfer using different analysis centre products for GNSSs. *Meas. Sci. Technol.* **2019**, *30*, 065003. [CrossRef]
34. Zhang, P.; Tu, R.; Gao, Y.; Zhang, R.; Han, J. Performance of Galileo precise time and frequency transfer models using quad-frequency carrier phase observations. *GPS Solut.* **2020**, *24*, 40. [CrossRef]
35. Zhang, P.; Tu, R.; Wu, W.; Liu, J.; Wang, X.; Zhang, R. Initial accuracy and reliability of current BDS-3 precise positioning, velocity estimation, and time transfer (PVT). *Adv. Space Res.* **2020**, *65*, 1225–1234. [CrossRef]
36. Lin, P.; Li, X.; Zhang, X.; Li, X.; Lu, C.; Zhao, Q.; Liu, J. Considering Inter-Frequency Clock Bias for BDS Triple-Frequency Precise Point Positioning. *Remote Sens.* **2017**, *9*, 734. [CrossRef]
37. Wang, J.; Huang, G.; Zhang, Q.; Gao, Y.; Gao, Y.; Luo, Y. GPS/BDS-2/Galileo Precise Point Positioning Ambiguity Resolution Based on the Uncombined Model. *Remote Sens.* **2020**, *12*, 1853. [CrossRef]
38. Wang, A.; Chen, J.; Zhang, Y.; Meng, L.; Wang, J. Performance of Selected Ionospheric Models in Multi-Global Navigation Satellite System Single-Frequency Positioning over China. *Remote Sens.* **2019**, *11*, 2070. [CrossRef]
39. Pan, L.; Zhang, X.; Liu, J.; Li, X.; Li, X. Performance evaluation of single-frequency precise point positioning with GPS, GLONASS, BeiDou and Galileo. *J. Navig.* **2017**, *70*, 465–482. [CrossRef]
40. Zhang, P.; Tu, R.; Gao, Y.; Hong, J.; Han, J.; Lu, X. Comparison of Multi-GNSS Time and Frequency Transfer Performance Using Overlap-Frequency Observations. *Remote Sens.* **2021**, *13*, 3130. [CrossRef]
41. Tu, R.; Zhang, R.; Zhang, P.; Han, J.; Fan, L.; Lu, X. Recover the abnormal positioning, velocity and timing services caused by BDS satellite orbital maneuvers. *Satell. Navig.* **2021**, *2*, 16. [CrossRef]